Structural, optical, and electrical analysis of tailoring $Bi_{2-x}Sb_xTe_3$ thin films

P. Chaiworn [a], S. Kaewja [a], E. Wongrat [b,c], C. Wichasilp [a], A. Tubtimtae [d*]
[a]*Department of Physics, Faculty of Science and Technology, Chiang Mai Rajabhat University, Chiang Mai, 50300, Thailand*
[b]*School of Science, University of Phayao, Phayao, 56000, Thailand*
[c]*Unit of Excellence on Sensors Technology, University of Phayao, Phayao, 56000, Thailand*
[d]*Division of Physics, Department of Physical and Material Sciences, Faculty of Liberal Arts and Science, Kasetsart University Kamphaeng Saen Campus, Nakhon Pathom 73140, Thailand*

Bismuth antimony telluride ($Bi_{2-x}Sb_xTe_3$) thin films were synthesized using chemical bath deposition (CBD) with various amounts of antimony. The structural, morphological, and optical properties of $Bi_{2-x}Sb_xTe_3$ thin films have been scrutinized using X-ray diffraction (XRD), field-emission scanning electron microscopy (FESEM), UV-Vis spectrophotometry. A higher amount of Sb contents can be observed the $Sb_{0.405}Te_{0.595}$, BiTe, and Bi_4Te_3 phases consisted in the pattern. Meanwhile, the energy band gaps are tuned in the range of 2.95 to 3.30 eV. Finally, measurement of resistance with various temperatures for activation energy (E_{AC}) estimation was performed. The highest E_{AC} value was equal to 0.654 eV for 0.8 g $SbCl_3$ as a precursor of Sb atom incorporated in the Bi_2Te_3 lattice.

(Received March 4, 2024; Accepted May 16, 2024)

Keywords: $Bi_{2-x}Sb_xTe_3$ thin film, Chemical bath deposition, Structural properties, Optical properties, Electrical properties

1. Introduction

In recent year, a V-VI ($A_2^VB_3^{VI}$) binary compound semiconductor in the form of thin film has been much intention for optoelectronic devices due to its stability and interesting unique characteristics. In case of bismuth telluride (Bi_2Te_3), it has a rhombohedral structure with space group $R\bar{3}m$. In the form of the layered structure, it exhibits strong anisotropic properties in the bulk form [1]. Previously, Bi_2Te_3 thin films have been preferred in optoelectronics, electrochemical devices, heat pumps infrared sensors, and photovoltaic solar cells [2]. While antimony telluride (Sb_2Te_3) is a narrow band gap and layered semiconductor with a tetradymite structure [3], mainly employed for minipower-generation systems and microcoolers, charge couple device (CCD), and infrared detectors [4]. However, the co-binary thin film has also been employed and considered for tuning their properties in practical applications. Previously, Bi_2Te_3/Sb_2Te_3 multilayers, synthesized using e-beam evaporation, have been investigated and provided excellent generating thermoelectric power and solid-state cooling [5]. Bi_2Te_3/Sb_2Te_3 films were deposited by a co-evaporation technique on substrates for the output performance of a thermoelectric generator (TEG) [6]. In addition, heterostructured Bi_2Te_3/Sb_2Te_3 thin film, synthesized using metal organic chemical vapor deposition (MOCVD) on a Si substrate, successfully employed in topological insulators (TIs) characterized by ideal topologically protected surface states based on spin-charge conversion (SCC) mechanisms [7]. As the background of above applications, Sb atom incorporated replacing Bi in Bi_2Te_3 to form a solid solution based on the Bi-Te binary alloy [8]. Thus, the changes the carrier type and concentration of the p-type Sb_2Te_3 thin film (E_g < 0.3 eV) were found to improve its properties of thin film [9].

* Corresponding author: tubtimtae@gmail.com
https://doi.org/10.15251/CL.2024.215.423

In this study, we synthesized the bismuth telluride thin film with various amounts of $SbCl_3$ to form bismuth antimony telluride ($Bi_{2-x}Sb_xTe_3$). Subsequently, structural, optical, and electrical properties of the as-prepared thin films were analyzed and investigated.

2. Experimental details

Initially, the borosilicate glass substrates were ultrasonically cleaned in nitric acid: methanol (3:7v/v), acetone, methanol, and deionized (DI) water for 10 min each. A 0.1 M Bi_2Te_3 powder (1.2 g) was dissolved in DI water (50 mL) with 1.0 g polyethylene glycol. Then, the solution was stirred at ambient temperature for 90 min. Afterwards, different weight amounts of $SbCl_3$ were added into the Bi_2Te_3 solution and stirred again at ambient temperature for 60 min. The glass substrates were then vertically dipped into the stirred mixing solution under 90 °C for 2 h. Then, the substrates were annealed at 120 °C for 5 min to form bismuth antimony telluride ($Bi_{2-x}Sb_xTe_3$) thin films. The samples were named as BAT-1, BAT-2, BAT-3, and BAT-4 for 0.6, 0.8, 1.2, and 2.4 g of $SbCl_3$, respectively. The structural properties were investigated by Rigaku Miniflex II X-ray diffractometer ($\lambda_{Cu\text{-}K\alpha}$ = 1.5406 Å). The surface and cross-sectional characteristics were observed by an UHR-SEM (TESCAN CLARA) and the compositional analysis was identified by an Oxford Ultim® Max energy dispersive X-ray spectroscope (EDS). Optical characteristics were investigated by a UV-Vis-NIR spectrometer (Varian Cary 50 Conc.). Finally, the resistance with various temperatures was recorded by a two-probe method of constantly interdigitated electrode through an insulator tester (FLUKE 1550 C).

3. Results and discussion

In Fig. 1(a), the prominent diffraction peak observed at $2\theta \approx 30.3°$ in the pattern of BAT-1 corresponding to the (222) and (004) for the cubic Bi_2O_3 (JCPDS: 045-1344) and orthorhombic Sb_2O (JCPDS: 011-0694) phases, respectively. The new reflection of small peak for BAT-2 to BAT-4 can be observed at $2\theta \approx 27.65°$ with the (230) and (104) planes of the monoclinic $Sb_{0.405}Te_{0.595}$ (JCPDS: 045-1229) and hexagonal BiTe (JCPDS: 075-1095) phases, respectively. Another peak was noticed in the patterns for BAT-3 and BAT-4, that is the (018) reflection plane at $2\theta \approx 29°$ of the rhombohedral Bi_4Te_3 phase (JCPDS: 075-1096). According to the size effect, the peaks for the sample BAT-2 to BAT-4 are not sharp and broaden hump, indicating the average crystallite size is small. In addition, broader hump and width become large in BAT-4 as the particles were smaller [10]. The peaks may have shifted with increasing Sb element due to the presence of varied crystallite sizes, their microstrain, and surface atom mobility [11]. The crystallite sizes are also calculated from Scherrer's formula and found approximately 12 nm and reduced to ~ 7 nm with increasing Sb amount.

Fig. 1(b-e) shows the surface and cross-sectional characteristics of BAT-1 to BAT-4. The thicknesses of the thin films ~ 450 – 2000 nm. As seen from the FESEM micrographs. The films have uniform and dense features for BAT-1 and BAT-2. Then, it became a rough granular surface with aggregated small particle distribution for BAT-3 where the high Sb content leads to the presence of a surface segregated layer because of Sb dissociative surface coverage [12]. However, flatted surface and uniform morphology with some cracks were performed for BAT-4. EDS analysis was also performed to investigate the elemental composition in the thin films. A higher Sb content was shown for BAT-1 to BAT-3, but lower for BAT-4. Possibly, the Sb amount has a threshold value of incorporation and greater saturation of Sb content may lead to dissolution of Sb ionic cation in the precursor and expected to decrease in Sb incorporation in the lattice [12].

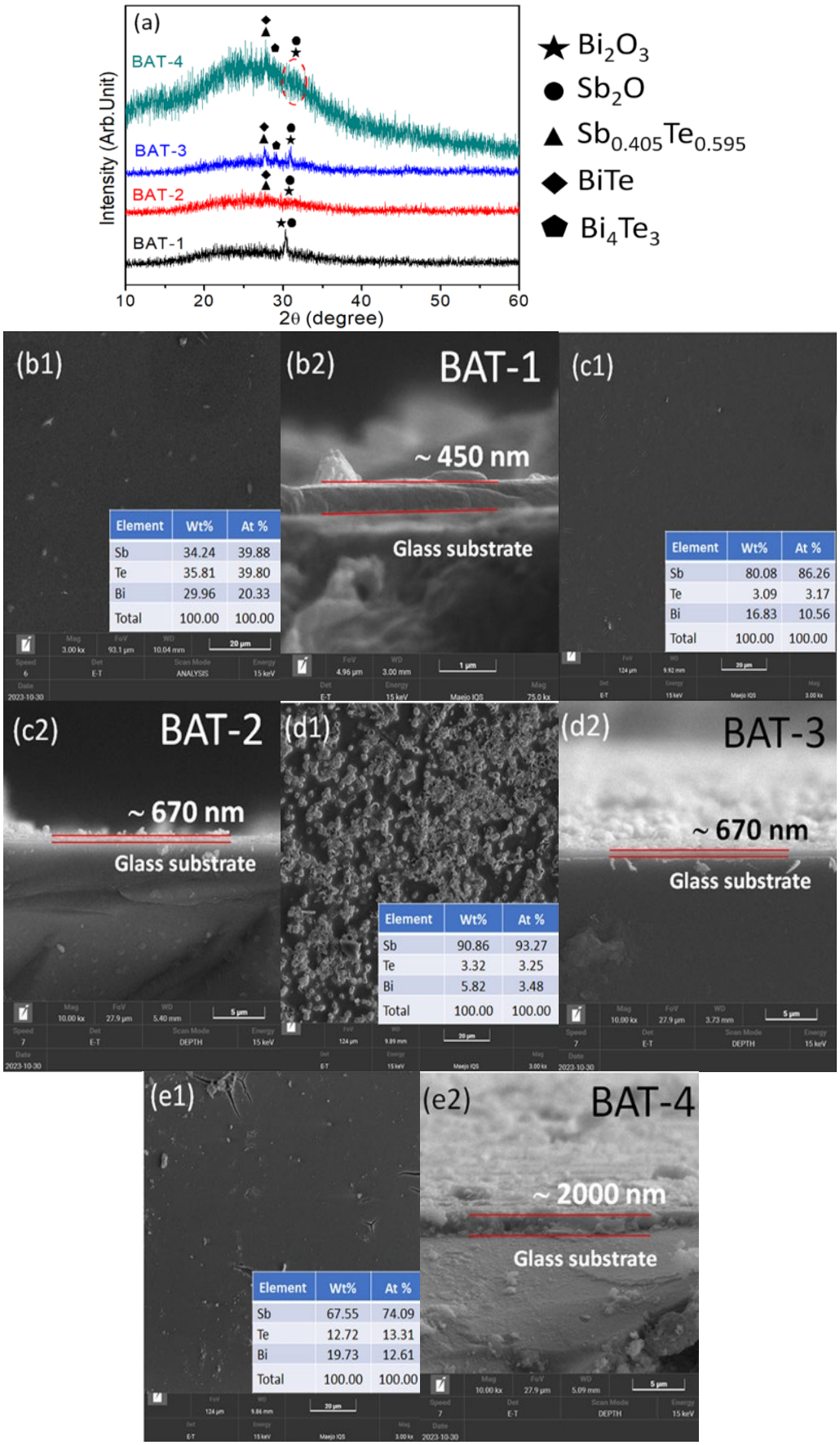

Fig. 1. (a) XRD patterns, (b-e) Surface and cross-sectional micrographs of the $Bi_{2-x}Sb_xTe_3$ thin films. (Inset: EDS spectra).

Fig. 2(a) displays the lower average transmittance ($T(\lambda)$) with increasing amount of $SbCl_3$ of 82.8%, 63.8%, 46.1%, and 35.2%, ranging of 400 – 1100 nm, possibly owing to the existence of high natural defect density [13]. In case of the reflectance ($R(\lambda)$) (Fig. 2(b)), the spectra are found to be reversed with average values of 1.14%, 3.00%, 5.85%, and 10.43%. The reflectance was employed using the Kubelka-Munk function [14]:

$$F(R) = \frac{(1-R)^2}{2R} = \frac{\alpha}{S}, \tag{1}$$

where α and S are absorption coefficient and scattering coefficient, respectively. As Eq. (1), the Tauc plot was expressed for the energy band gap (E_g) determination of the samples [14]:

$$[F(R) \cdot hv]^2 = A(hv - E_g) \tag{2}$$

Meanwhile, h, v, and A are the Planck's constant, light frequency, and proportionality constant, respectively. In Fig. 2(c-f), the overall decrease in E_g for BAT-2 (2.95 eV) to BAT-4 (3.00 eV), compared with BAT-1 (3.30 eV), attributes to defects since Sb^{3+} substitute into Bi_2Te_3 host lattice, but slightly increasing E_g for these sample conditions corresponded to Burstein-Moss effect associated with increased carrier concentration and imperfection in polycrystalline thin films [15].

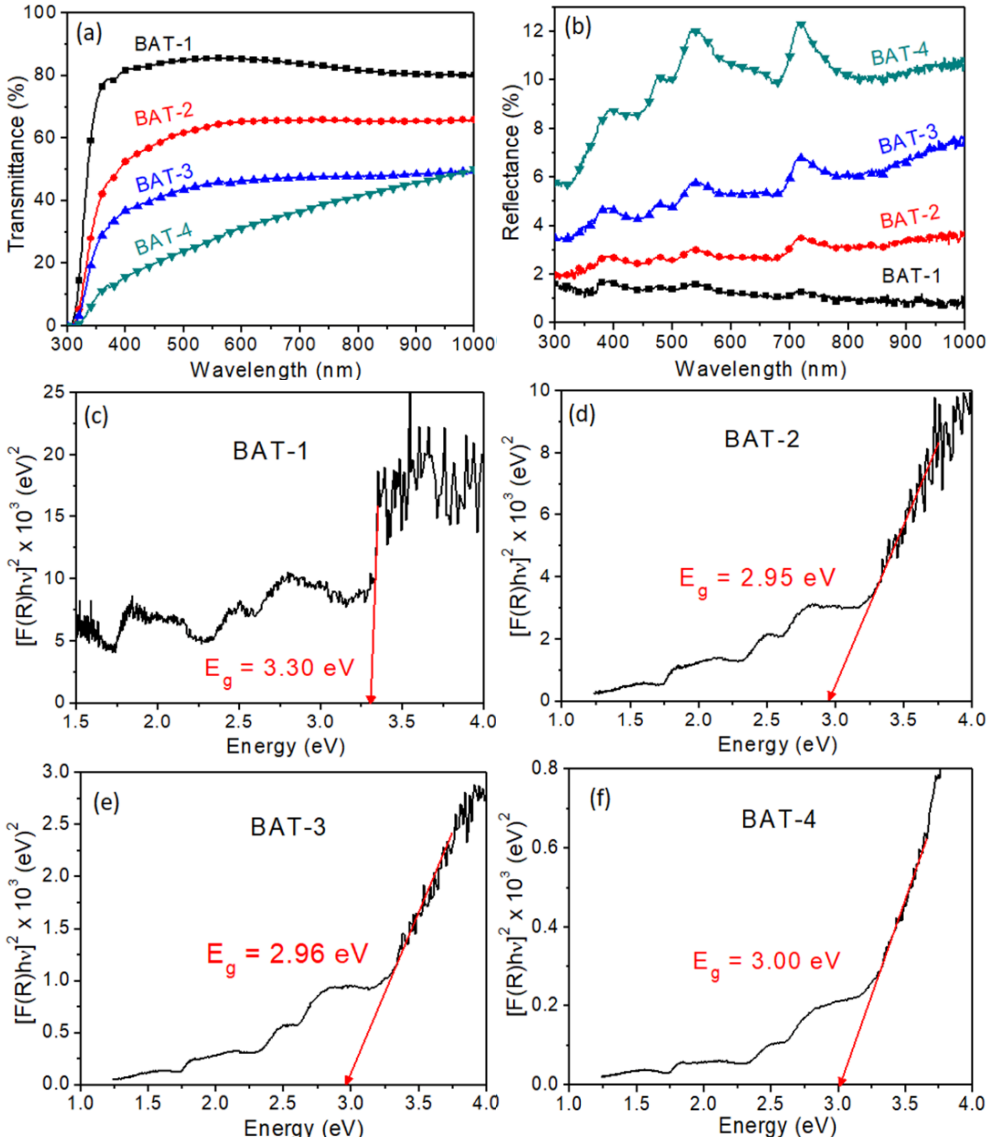

Fig. 2. (a) Transmittance, (b) Reflectance, and (c-f) Tauc's plot analysis for energy band gap determination.

This leads to shifted Fermi level to higher energy [16]. Furthermore, the decrease in crystallite size (increase in crystallite boundaries) with amorphous formation and occurred electronic Schottky barrier at the boundaries are also plausible for the increase in E_g due to quantum confinement effect especially in the sample BAT-3 (2.96 eV) and BAT-4 (3.00 eV) [17].

Fig. 3 displays the alteration in the resistance with absolute temperature for the prepared samples. As the semiconducting nature of the samples, the resistance decreased with increasing temperature [18]. The resistance values at room temperature (298.15 K) are 147, 402, 1080, and 169 MΩ for BAT-1 to BAT-4, respectively. The resistivity (ρ) and conductivity (σ) can be calculated with the thickness (t) of the thin films by the relations [19]:

$$\rho = \frac{\pi}{ln2} \times t \times R = 4.53236 \times t \times R \tag{3}$$

and

$$\sigma = \frac{1}{\rho} \tag{4}$$

The ρ values are 0.3 × 10^3, 1.22 × 10^3, 3.28 × 10^3, and 1.53 × 10^3 Ω·m with σ = 3.34 × 10^{-3}, 0.819 × 10^{-3}, 0.305 × 10^{-3}, and 0.653 × 10^{-3} $(\Omega \cdot m)^{-1}$, respectively.

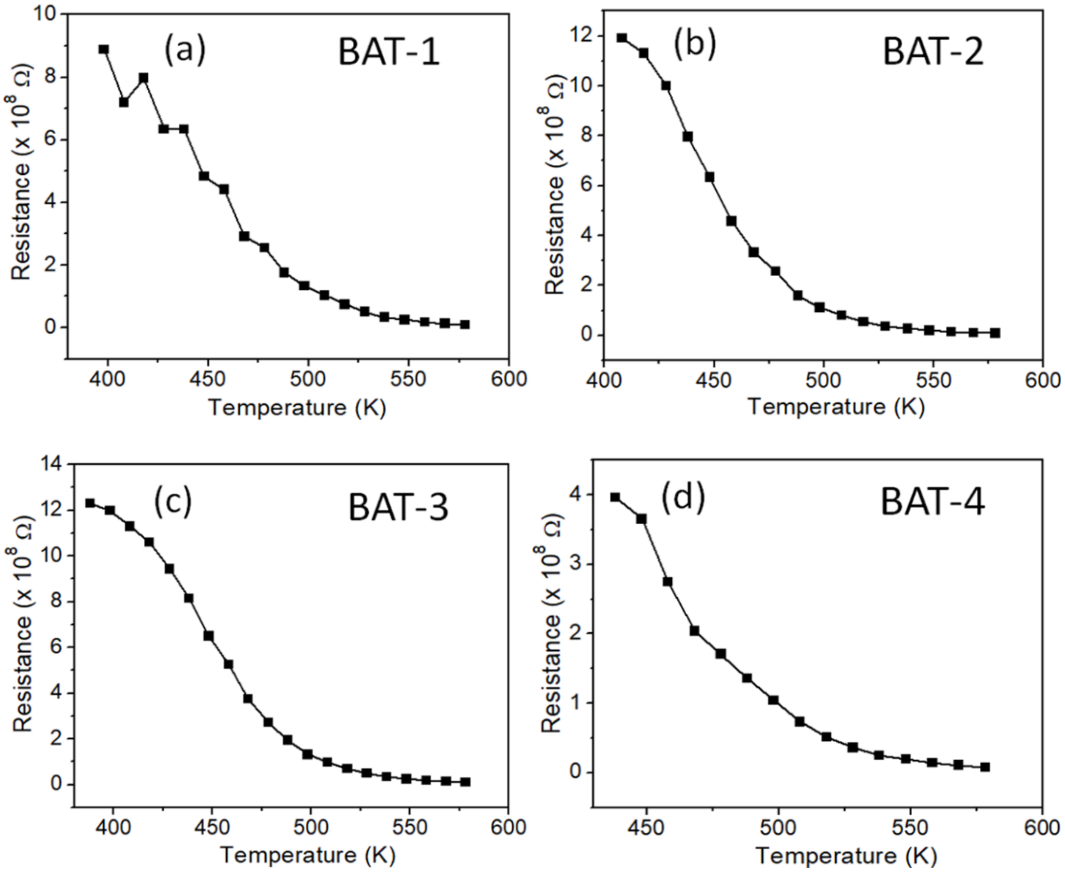

Fig. 3. Variation of resistance vs. temperature for the $Bi_{2-x}Sb_xTe_3$ thin films.

Fig. 4(a-d) show the plots of $\ln(\sigma)$ vs. $1000/T$ for the $Sb_xBi_{2-x}Te_3$ thin films. The activation energy (E_{AC}) was determined by the slope of the linear fit according to the Arrhenius formula [20]:

$$\sigma = \sigma_0 \exp\left(\frac{-E_{AC}}{k_B T}\right), \tag{5}$$

or

$$ln(\sigma) = ln(\sigma_0) - \frac{E_{AC}}{8.617\times10^{-2}} \times \frac{1000}{T} \tag{6}$$

σ_0 depicts the pre-exponential factor, E_{AC} is the activation energy of the conduction mechanism and k_B represents Boltzmann's constant. The E_{AC} values were equal to 0.516, 0.654, 0.534, and 0.635 eV for BAT-1 to BAT-4, respectively. Our result of E_{AC} for the $Sb_xBi_{2-x}Te_3$ thin films is close to the $Na_2B_4O_7$ glass system (E_{AC} = 0.64 eV) [21] and the $Cd_{1-x}Hg_xTe$ thin film synthesized by a chemical bath deposition (CBD) method (E_{AC} ~ 0.514 eV) [22].

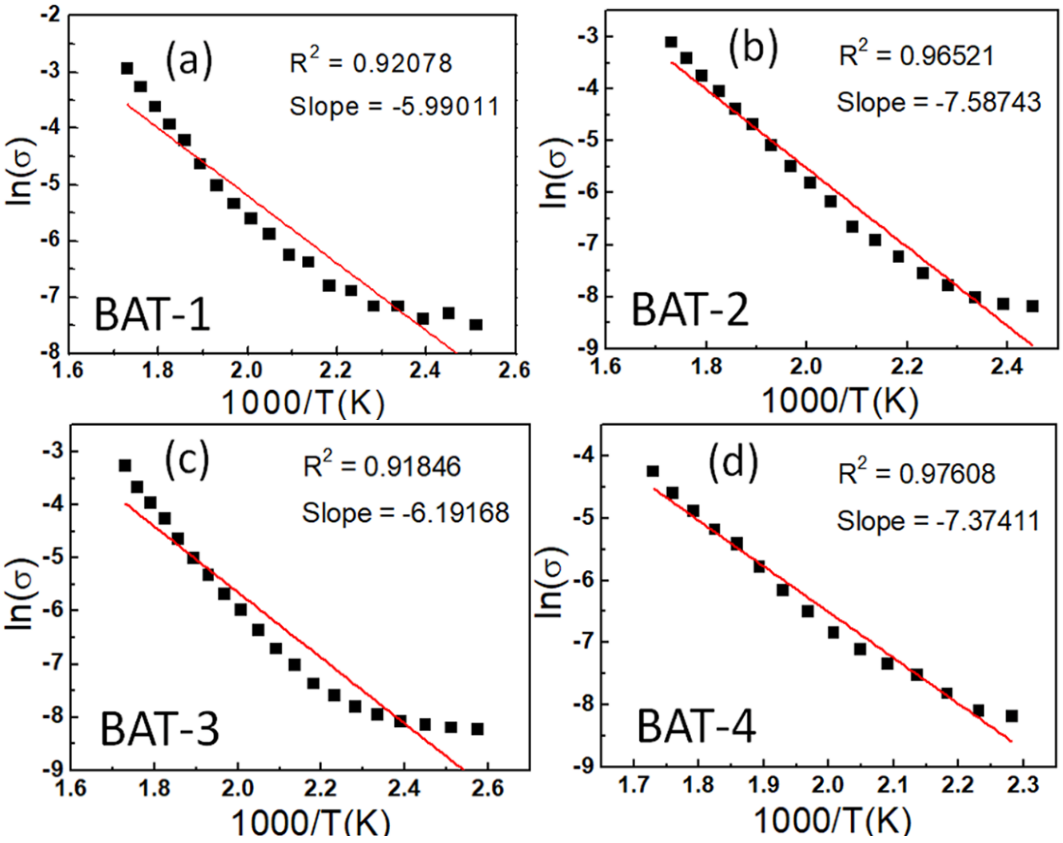

Fig. 4. Plots of ln(σ) vs. 1000/T of the $Bi_{2-x}Sb_xTe_3$ thin films.

4. Conclusion

The $Bi_{2-x}Sb_xTe_3$ thin films have been synthesized using a chemical bath deposition method. The prominent peak for binary chalcogenides were $Sb_{0.405}Te_{0.595}$ and BiTe with higher Sb content. The crystallite sizes are found approximately 12 nm and reduced to ~ 7 nm with increasing Sb amount. In other hand, the dissolution of Sb ionic cation in the precursor leads to expect decreasing in Sb incorporation in the lattice. Finally, the highest σ and E_{AC} values was equal to 3.34×10^{-3} $(\Omega\cdot m)^{-1}$ and 0.654 eV for 0.6 and 0.8 g $SbCl_3$ as a precursor of Sb atom incorporated in the lattice, respectively.

Acknowledgments

This work was supported by Chiang Mai Rajabhat University and the Unit of Excellence on Sensors Technology, School of Science, University of Phayao, Thailand, while the proofreading service was funded and supported by Kasetsart University, Kamphaeng Saen Campus, Thailand.

References

[1] C. Sudarshan, S. Jayakumar, K. Vaideki, C. Sudakar, Thin Solid Films **713**, 138355 (2020); https://doi.org/10.1016/j.tsf.2020.138355
[2] A. M. Adam, J. Alloys Compd. **765**, 1072 (2018); https://doi.org/10.1016/j.jallcom.2018.06.159
[3] S. Shi, M. Cao, C. Hu, Cryst. Growth Des. **9**, 2057 (2009); https://doi.org/10.1021/cg800551u
[4] P. Christian, P. O'Brien, J. Mater. Chem. **15**, 4949 (2005); https://doi.org/10.1039/B511952A
[5] Z. Xiao, K. Kisslinger, E. Dimasi, J. Kimbrough, Microelectron. Eng. **197**, 8 (2018); https://doi.org/10.1016/j.mee.2018.05.001
[6] E. M. F Vieira, A.L. Pires, J. P. B. Silva, V. H. Magalhães, J. Grilo, F. P. Brito, M. F. Silva, A. M. Pereira, L. M. Goncalves, ACS Appl. Mater. Interfaces **11**, 38946 (2019); 10.1021/acsami.9b13254
[7] E. Longo, L. Locatelli, P. Tsipas, A. Lintzeris, A. Dimoulas, M. Fanciulli, M. Longo, R. Mantovan, ACS Appl. Mater. Interfaces **15**, 50237 (2023); 10.1021/acsami.3c08830
[8] S. I. Kim, S. Hwang, J. W. Roh, K. Ahn, D. H. Yeon, K. H. Lee, S. W. Kim, J. Mater. Res., **27**, 2449 (2012); https://doi.org/10.1557/jmr.2012.273
[9] G.S. Nolas, J. Sharp, J. Goldsmid, Thermoelectrics: Basic Principles and New Materials Developments, Springer-Verlag Berlin Heidelberg, New York (2013) 123.
[10] A. A. Prema, R. J. Xavier, A. S. Dawood, P. A. Sahayaraj, C. Pragathiswaran, A. J. Amalraj, V. Dharmalingam, Der Pharma Chem. **8**, 96 (2016).
[11] B. Z. Bhari, K. S. Rahman, P. Chelvanathan, M. A. Ibrahim, Mater. Lett. **339**, 134097 (2023); https://doi.org/10.1016/j.matlet.2023.134097
[12] Z. Zhang, K. Ghosh, N. N. Faleev, H. Wang, C. B. Honsberg, P. Reece, S. P. Bremner, J. Cryst. Growth **526**, 125231 (2019); 10.1016/j.jcrysgro.2019.125231
[13] H. Suarez, J. M. Correa, S. D. Cruz, C. A. Otalora, M. Hurtado, G. Gordillo, 2013 IEEE 39th Photovoltaic Specialists Conference (PVSC), Tampa, FL, USA (2013) 2585.
[14] Ch. L. Rajesh, R. N. Madhusudhana, Optik **294**, 171472 (2023); https://doi.org/10.1016/j.ijleo.2023.171472
[15] D. Bao, H. Gu, A. Kuang, Thin Solid Films **312**, 37 (1998); https://doi.org/10.1016/S0040-6090(97)00302-7
[16] R. Nouadji, A. Attaf, A. Derbali, A. Bouhdjer, N. Saidi, M. S. Aida, F. Zeribi, O. Benkhetta, R. Messemeche, M. Nouadji, N. Attaf, Main Group Chem. **20**, 513 (2021); 10.3233/MGC-210063
[17] J. Sawahata, M. M. Islam, Thin Solid Films **752**, 139249 (2022); https://doi.org/10.1016/j.tsf.2022.139249
[18] P. A. Chate, S. D. Lakde, D.J. Sathe, Optik **250**, 168296 (2022); https://doi.org/10.1016/j.ijleo.2021.168296
[19] M. Ghougali, O. Belahssen, S. Benhamida, M. Mimouni, G. Rihia, M. S. Mahboub, A. Beggas, Chalcogenide Lett. **18**, 765 (2021); https://doi.org/10.15251/CL.2021.1812.765
[20] A. Qasem, N. M. Said, A. A. Hassan, H. A. Yakout, E. R. Shaaban, Phys. B: Condens. Matter **627**, 413600 (2022); https://doi.org/10.1016/j.physb.2021.413600
[21] A. A. Kutub, F. Gouda, AIP Conf. Proc. **1370**, 149 (2011); https://doi.org/10.1063/1.3638096
[22] B. R Arbad, S. G. Chonde, P .P. Hankare, V. M. Bhuse, Chemical deposition of (CdHg)Te ternary thin films, Arch. Appl. Sci. Res. **3**, 422 (2011).